



Silver-polymer core-shell nanoparticles for ultrastable plasmon-enhanced photocatalysis



Ramesh Asapu^a, Nathalie Claes^b, Sara Bals^b, Siegfried Denys^a, Christophe Detavernier^c, Silvia Lenaerts^a, Sammy W. Verbruggen^{a,d,*}

^a Sustainable Energy, Air and Water Technology (DuEL), Department of Bioscience Engineering, University of Antwerp, Groenenborgerlaan 171, Antwerp 2020, Belgium

^b Electron Microscopy for Material Science (EMAT), Department of Physics, University of Antwerp, Groenenborgerlaan 171, Antwerp 2020 Belgium, Belgium

^c Department of Solid State Science, Ghent University, Krijgslaan 281/S1, Gent 9000, Belgium

^d Center for surface Chemistry and Catalysis, Department of Microbial and Molecular Systems, KU Leuven, Celestijnenlaan 200f, Leuven 3001, Belgium

ARTICLE INFO

Article history:

Received 10 May 2016

Received in revised form 20 June 2016

Accepted 25 June 2016

Available online 27 June 2016

Keywords:

Photocatalysis

Surface plasmon resonance (SPR)

Layer-by-layer (LbL)

Silver

Core-shell

Stability

ABSTRACT

Affordable silver-polymer core-shell nanoparticles are prepared using the layer-by-layer (LbL) technique. The metallic silver core is encapsulated with an ultra-thin protective shell that prevents oxidation and clustering without compromising the plasmonic properties. The core-shell nanoparticles retain their plasmonic near field enhancement effect, as studied from finite element numerical simulations. Control over the shell thickness up to the sub-nanometer level is there for key. The particles are used to prepare a plasmonic Ag-TiO₂ photocatalyst of which the gas phase photocatalytic activity is monitored over a period of four months. The described system outperforms pristine TiO₂ and retains its plasmonic enhancement in contrast to TiO₂ modified with bare silver nanoparticles. With this an important step is made toward the development of long-term stable plasmonic (photocatalytic) applications.

© 2016 Elsevier B.V. All rights reserved.

1. Introduction

The application of plasmonic nanoparticles has found its way in different areas of research such as solar cells [1], plasmonic photocatalysis [2–7], surface-enhanced Raman scattering (SERS) [8] and biophotonics [9]. Among those noble metals that exhibit surface plasmon resonance (SPR), gold and silver are most commonly investigated as they display SPR over a wide wavelength range and their SPR properties can easily be tuned through their size, shape and (alloy) composition [3,10]. The synthesis of stable (functionalized) plasmonic nanoparticles is of high importance as they carry unique surface properties with applications in various research domains, e.g. encapsulation of plasmonic nanoparticles is of particular interest to biomedical science with applications in drug delivery [11] and imaging [12]. Overall, gold nanoparticles are more stable and easy to functionalize, explaining the major literature focus on this type of metal. Functionalization of

gold nanoparticles using thiols and ligands capping the nanoparticles [13], as well as encapsulation using polyelectrolytes has been documented well [14–16]. In contrast, functionalization of silver nanoparticles is less obvious, as it is challenging with respect to stability, aggregation and size control. Also, silver nanoparticles are prone to oxidation when left over prolonged periods, which hinders functionalizing the surface. A solution to these challenges is the preparation of stable silver nanoparticles with a core-shell structure consisting of a silver core surrounded by a thin protective shell that prevents oxidation of the silver nanoparticle. In the context of silver encapsulation, the use of organic linkers (e.g. thiol-derivatives, xanthate, etc.) [17–19] has been reported as well as various (mostly one-pot) synthesis strategies for capping with inorganic shells (e.g. silica, inorganic carbon) [20–23]. The main drawback in all of these aforementioned methods is that they do not present complete freedom to accurately control the shell thickness, though this is one of the most crucial parameters in many plasmonic applications such as SERS [12], where slight changes in shell thickness can alter the near field enhancement to a large extent. The Layer-by-Layer (LbL) method is a simple yet powerful technique to apply ultra-thin shells on colloidal templates [15,24]. Fabrication of silver core-shell nanoparticles using the LbL method has

* Corresponding author at: Sustainable Energy, Air and Water Technology (DuEL), Department of Bioscience Engineering, University of Antwerp, Groenenborgerlaan 171, Antwerp 2020, Belgium.

E-mail address: sammy.verbruggen@uantwerp.be (S.W. Verbruggen).

only been reported on silver nanocubes by prior functionalization of the surface using surfactants and washing with buffers during the layer deposition process [25]. In this work, the LbL method is directly applied to as-prepared spherical silver nanoparticles without the use of any additional surfactants or supporting layers, this way avoiding supplementary washing steps with buffers. Preparing silver-core polymer-shell nanoparticles in such fashion is a facile and versatile strategy with the freedom to control the shell thickness at the nanoscale, typically even less than one nanometer. Furthermore, we succeeded in performing the synthesis with the less expensive negatively charged polyelectrolyte, polyacrylic acid (PAA), in contrast to the more expensive poly(styrene sulfonate) (PSS) which is traditionally used for nanoscale colloidal systems, in combination with the positively charged polyelectrolyte poly(allylamine hydrochloride) (PAH). The main objectives of this work are to study (i) the effect of the polymer shell on the plasmonic field enhancement properties and (ii) the stability of the resulting capped silver nanoparticles when deposited on TiO_2 for photocatalytic environmental remediation. More in particular the plasmon-enhanced photocatalytic degradation of acetaldehyde, a common hazardous indoor air pollutant, is studied. In such systems the silver core-shell nanoparticles serve a dual purpose: (i) the polymer shell protects the silver nanoparticle from oxidation and clustering and (ii) the SPR properties of silver create intense local electric fields that enhance the charge carrier generation and thus improve the photocatalytic acetaldehyde degradation reaction.

2. Experimental section

2.1. Synthesis of silver-polymer core shell nanoparticles

Stock solutions of polyelectrolytes polyallylamine hydrochloride (PAH, MW 17.5 KDa Sigma-Aldrich), polyacrylic acid (PAA, MW 2 KDa Sigma-Aldrich) and poly(styrene sulfonate) sodium salt (PSS, MW 15 KDa Polymer Standard Services GmbH) were prepared in Milli-Q water by sonication for 30 min and used as required. 12 mL of the as prepared silver colloidal solution (procedure reported elsewhere [26]) was centrifuged at 8000 rpm for 100 min and redispersed in Milli-Q water. This was done to remove most of the citrate in the colloidal silver solution, in order to reduce the interference of charge on the citrate molecule and to have optimal deposition of the first polycation layer (PAH). 12 mL of this centrifuged silver colloidal solution was added dropwise to 6 mL of 5 g/L PAH solution under vigorous stirring in a glass vial. The stirring was continued at room temperature for 20 min in dark. The resulting colloidal solution was centrifuged in 1.5 mL Eppendorf tubes to remove the excess polyelectrolyte. Around 1460–1480 mL of supernatant was discarded and the remaining dark-brownish gel-like pellet was redispersed in Milli-Q water. The centrifuge process was repeated one more time as a washing step and the final redispersion in Milli-Q water was adapted to obtain 12 mL of colloid. A small aliquot of this PAH coated silver colloid sample was stored for characterization purposes and the deposition of the second layer i.e. polyanion PAA (10 g/L) was continued using the same procedure as described above. The centrifuge speed was slightly adapted after each deposition step to avoid formation of hard pellets that cannot be redispersed.

2.2. Photocatalytic activity tests

The Ag- TiO_2 plasmonic photocatalytic system was prepared with a 5 wt.% suspension of commercial TiO_2 (P25, Evonik) nanoparticles in ethanol and stirred ultrasonically. 100 μL of the suspension was spin coated at 1500 rpm for 60 s onto several piranha cleaned glass slides of 1.5 cm \times 2.5 cm. The substrates were

dried overnight at 100 °C followed by spin coating with 75 μL of the colloidal solution of bare silver or silver-polymer core-shell nanoparticles at 1500 rpm and finally air dried at 80 °C for 6 h. Two identical slides were used to perform one photocatalytic test. As such, three different samples were prepared: a pristine P25 reference film; a P25 film coated with bare silver nanoparticles, denoted P25_Ag; and a P25 film coated with four layered core-shell silver nanoparticles, denoted P25_Ag_L4. The photocatalytic activity of above prepared films is measured online by monitoring the gas phase degradation of acetaldehyde under UVA irradiation in a glass slit reactor using FTIR detection. Measurements are repeated over a period of 16 weeks in order to study the stabilizing effect offered by the protective shell. The reactor design, set-up and operation is explained in detail in previous work of our research group [27–32].

2.3. Characterization

Spectroscopy measurements were performed with a Shimadzu 2501 spectrophotometer in a UV-cuvette of 10 mm path length to locate the SPR peak. Scans were performed in the spectral range of 300–800 nm with a resolution of 0.2 nm and an average of three measurements was taken. Zeta potential measurements were done using Brookhaven's ZetaPlus zeta potential analyzer to monitor the surface charge on the core-shell nanoparticles. A FEI Tecnai Transmission Electron Microscope (TEM) operated at 200 kV was used to visualize the core-shell structure of nanoparticles. In a typical procedure 20 μL of the colloidal solution was absorbed during 5 min on a quantifoil copper grid coated with a 3.19 nm carbon film. For HAADF-STEM measurements, spin coated material (as described in 2.2) was scraped off the glass substrate and dispersed in ethanol before sampling.

3. Results and discussions

3.1. Silver-Polymer core-shell nanoparticles through LbL

Silver nanoparticles with diameter around 18 nm were synthesized by reduction of silver nitrate with tannic acid and trisodium citrate as described elsewhere [26]. Silver-polymer core shell nanoparticles are prepared by the LbL method, i.e. sequential cycles of adsorption and washing of alternatively charged polyelectrolytes. The alternate deposition of polycation and polyanion chains was continued until the desired number of layers was obtained that results in the encapsulation of the silver core by a thin polymer shell. Zeta potential measurements after each adsorption cycle show the inversion of surface charge on the core-shell nanoparticles with the deposition of alternatingly charged polyelectrolytes, evidencing the success of the LbL strategy (Fig. 1a). The UV-vis absorption spectrum of the core-shell nanoparticles was also recorded after each deposition step (Fig. 1b). By measuring the absorption intensity, it could be determined that on average 85% of silver nanoparticles was retained after each deposition cycle, which is in line with an optimized LbL procedure on gold nanoparticles [16]. A clear red shift of the SPR peak with increasing number of adsorbed layers can also be observed in Fig. 2a, which indicates the gradual increase in particle size as more LbL layers are added. Traditionally, the strong – yet expensive – polyelectrolyte PSS is used as the polyanion in the LbL synthesis. At the beginning of our study, we have investigated the possibility of replacing PSS by the weaker but cheaper low-molecular weight PAA polyanion. For comparison purposes, two sets of silver-polyelectrolyte systems were prepared, i.e. with PAH/PAA and PAH/PSS. As seen from Fig. 2b, the SPR peak red shift for silver nanoparticles using the polyelectrolyte system of PAH/PSS shows similar behavior when compared to the PAH/PAA polyelectrolyte system. Also the cor-

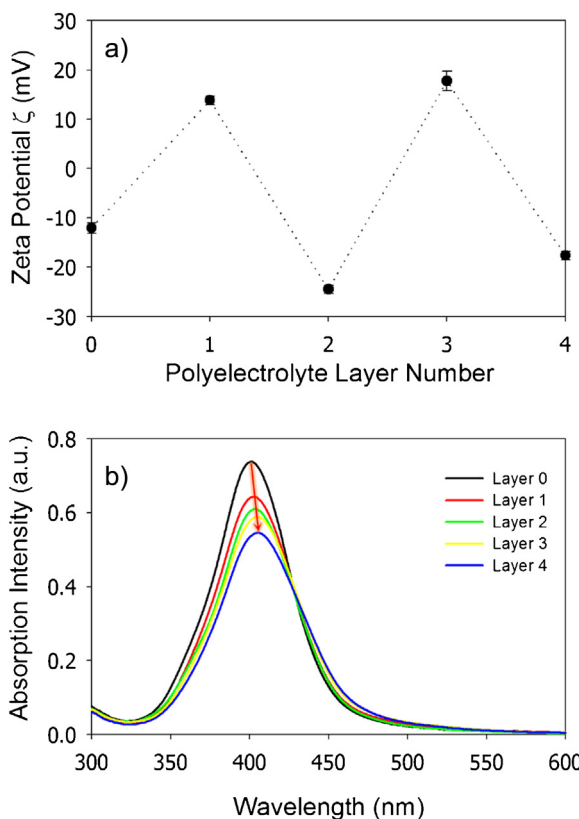


Fig. 1. a) Zeta potential of core-shell silver nanoparticles $\text{Ag}/(\text{PAH}/\text{PAA})_2$ as a function of adsorbed polyelectrolyte layer. b) UV-vis absorption spectra of core-shell silver nanoparticles as a function of adsorbed polyelectrolyte layer. The red arrow indicates the red shift in SPR peak position. (For interpretation of the references to colour in this figure legend, the reader is referred to the web version of this article.)

responding shell thicknesses are similar (Fig. 3), confirming the feasibility of using PAA as the polyanion for the LbL synthesis as a cost-effective alternative to PSS. From the UV-vis spectrophotometric measurements, it may be inferred that the red shift of the SPR peak after the first four layers is comparatively less signifi-

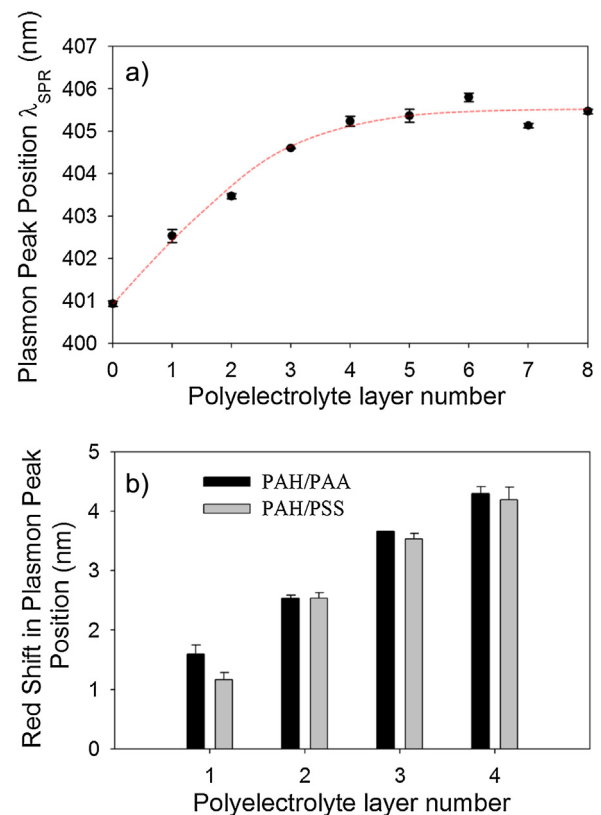


Fig. 2. a) Plasmon peak position of the silver core-shell nanoparticles as a function of number of adsorbed PAH/PAA polyelectrolyte layers. b) Comparison of red shift in SPR peak position in different polyelectrolyte systems PAH/PAA and PAH/PSS.

cant, though an increase in shell thickness is confirmed by the TEM images in Fig. 3. As seen from these images (Fig. 3a and b), the four- and eight-layered core-shell nanoparticles, denoted as Ag_L4 and Ag_L8 , are encapsulated by a thin shell of thickness (1.4 ± 0.4) nm and (2.4 ± 0.7) nm respectively, as derived from 100 shell thickness measurements in TEM. This demonstrates the continuous growth of the shell with increasing number of polyelectrolyte layers. During

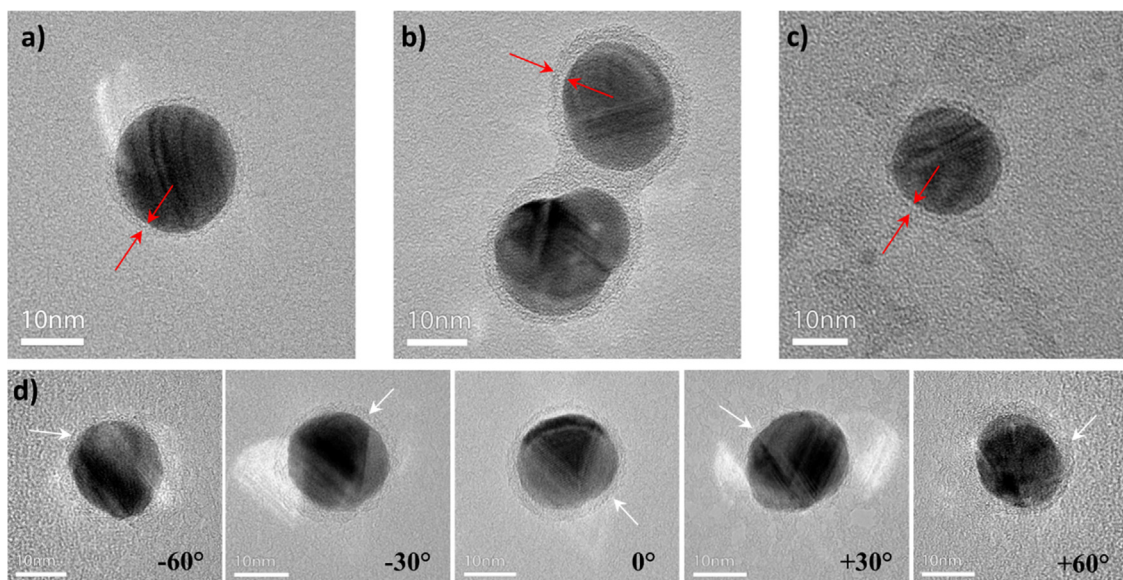


Fig. 3. Silver core-shell nanoparticles with silver core and an ultrathin shell composed of a) four polyelectrolyte layers (Ag_L4) $\text{Ag}/(\text{PAH}/\text{PAA})_2$ of thickness 1.4 ± 0.4 nm, b) eight polyelectrolyte layers (Ag_L8) $\text{Ag}/(\text{PAH}/\text{PAA})_4$ of thickness 2.4 ± 0.6 nm, c) four polyelectrolyte layers (Ag_L4) $\text{Ag}/(\text{PAH}/\text{PSS})_2$ of thickness 1.6 ± 0.4 nm, d) TEM tilt series of Ag_L8 core-shell nanoparticles. All the inset bars represent a scale of 10 nm. The shell thickness distribution is based on 100 measurements.

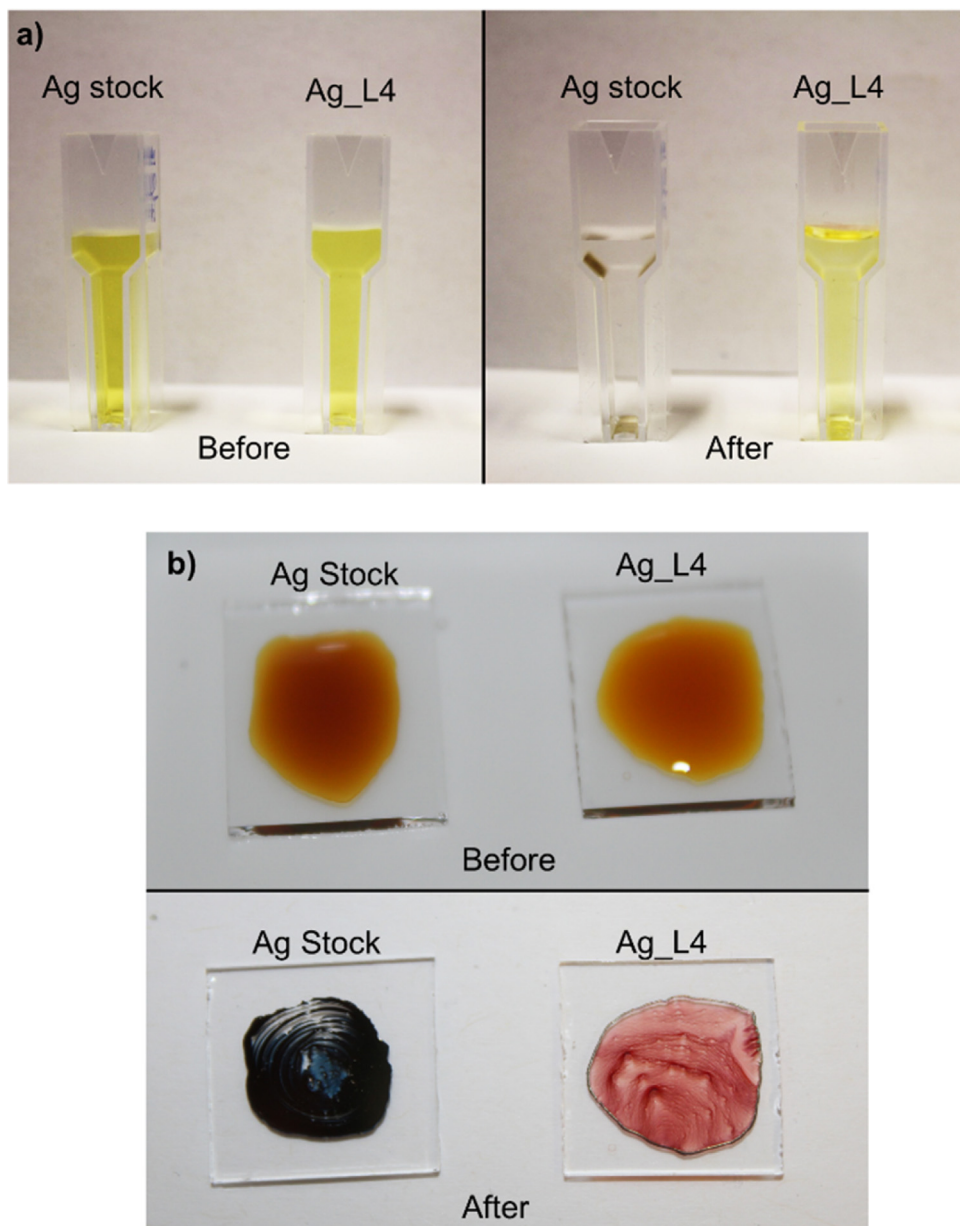


Fig. 4. a) Photographic images showing the effect of salt addition on unprotected Ag versus protected Ag_L4 colloidal nanoparticles and b) Photographic images showing the effect of hot air treatment on unprotected Ag versus protected Ag_L4 nanoparticles.

TEM analysis the particles were also tilted over a series of different angles. The shell can be clearly observed from every projection, evidencing the silver particles are completely and homogeneously covered by the polyelectrolytes (Fig. 3d).

As previously mentioned, our intention is to use these plasmonic nanoparticles in a gas phase photocatalytic system in an oxidative atmosphere (acetaldehyde in air). It is therefore crucial to *a priori* evaluate the stability of the prepared nanoparticles in order for this approach to succeed. Also other plasmon-based application such as SERS and most of bio-sensing applications heavily depend on the stability of the nanoparticle system in stressful conditions. The latter application, for instance, requires colloidal stability in the presence of salt buffers. Hence, as a first test, the stability of the as-prepared silver and silver-polymer core-shell colloidal nanoparticles was studied upon addition of sodium chloride salt. To 1.5 mL of colloidal solution of unprotected Ag and protected Ag_L4 nanoparticles, 150 μ L of 1 M NaCl solution was added and an immediate color change was observed for bare Ag nanoparticles

whereas the core-shell nanoparticles retained their bright yellow color showcasing the stability and resistance of the polymer shell to the permeation of chloride ions as seen from Fig. 4a. For the bare silver colloidal solution, dark precipitates are observed at the bottom of the test vial after the solutions were aspirated and allowed to stand overnight.

A second stability test consisted of subjecting the colloidal nanoparticles to a harsh hot-air treatment. Keeping in mind the photocatalytic application of acetaldehyde degradation, this test will already reveal the potential of the nanoparticles to resist harsh oxidative conditions. For this test colloidal solutions of unprotected Ag and protected Ag_L4 nanoparticles were concentrated by centrifugation and drop casted on cleaned quartz substrates. Initially both the concentrated unprotected Ag and Ag_L4 nanoparticles have a similar orange-like color as seen from Fig. 4b. After the heat treatment at 105 °C overnight in the presence of air, a drastic color change from to greyish black is observed for unprotected silver nanoparticles, which is characteristic of silver oxide. On the

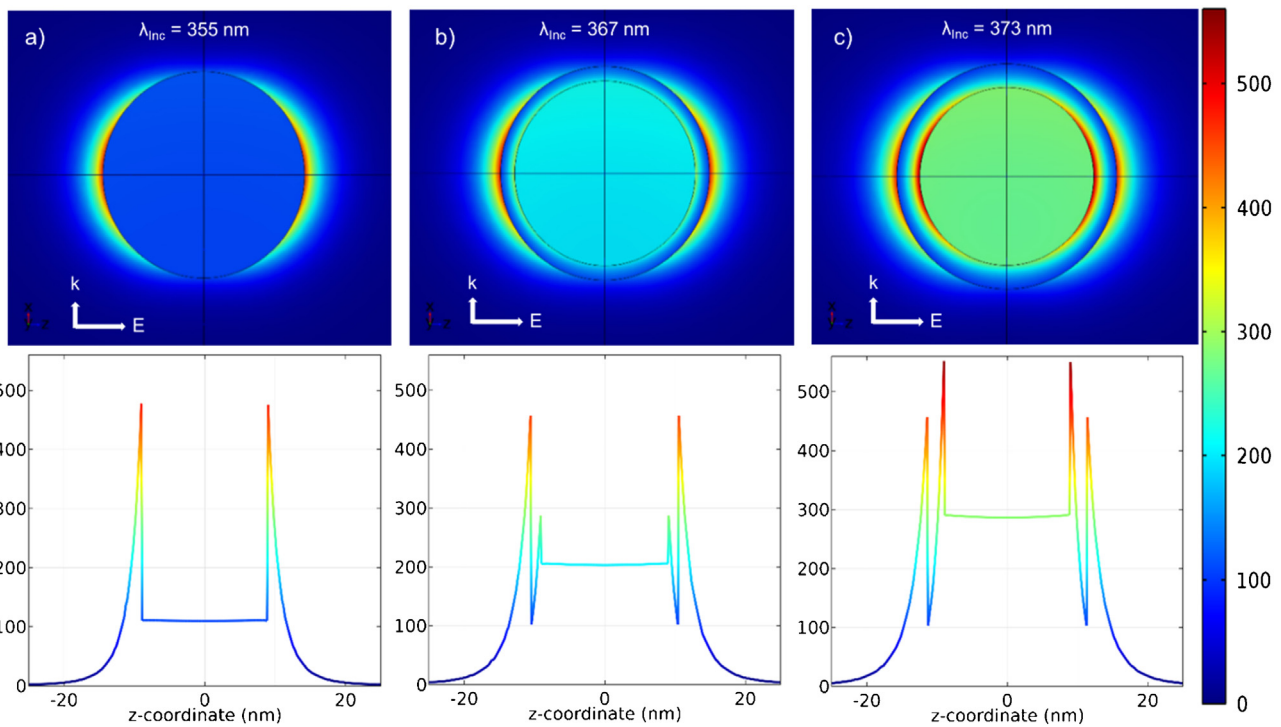


Fig. 5. Electric field distribution maps ($|E|/|E_0|$)² for a) bare silver nanoparticle, b) silver encapsulated by a polymer shell of thickness 1.4 nm, alike Ag.L4 and c) silver encapsulated by a polymer shell of thickness 2.4 nm, alike Ag.L8. The field enhancement along the Z-axis, i.e. in the direction of polarization, is plotted below the corresponding field maps.

other hand the silver-polymer core-shell nanoparticles Ag.L4 retain the orange color showcasing their ultrastable nature. This proves that the polymer shell is acting as a protective barrier for silver nanoparticles against oxidation and will help retaining the plasmonic properties.

3.2. Near-field enhancement studies

The effect of the polymer shell on the plasmonic near field enhancement of the silver nanoparticles is studied by a finite element analysis using wave optics physics in COMSOL Multiphysics (version 5.1). To represent the bare silver nanoparticle, a 3D sphere of 18 nm in diameter was built and a shell was added on the silver core with varying thickness to represent the polymer shell. The optical data for silver was taken from Johnson and Christy [33] and the refractive index of the polymer shell system ($n = 1.48$) was taken from literature [34]. The polymer domain was meshed using a custom setting for a maximum element size of 1 nm and all the models had at least 105 tetrahedral elements with mesh quality varying from 0.7–0.75. Air is taken as the surrounding medium and a plane wave polarized in the Z-axis direction and propagating along the X-axis direction was used for solving the scattered field of Maxwell's wave equations in a wavelength domain study. Fig. 5 shows the normalized electric field enhancement ($|E|/|E_0|$)² emanating from the surface of a 18 nm bare silver nanoparticle, this silver particle encapsulated by a polymer shell of thickness 1.4 nm (alike Ag.L4) and finally the silver particle encapsulated by a polymer shell of thickness 2.4 nm (alike Ag.L8). The color map represents the normalized electric field intensity distribution visualized on the ZX plane. An incident monochromatic plane wave propagating along the X-axis and polarized along the Z-axis with $\lambda_{\text{Incident}} = \lambda_{\text{SPR}}$ (taking into account the red shift with increasing layer thickness) for each nanoparticle system is used for the numerical simulations. This means the incident excitation wavelength of the monochromatic plane wave was always kept the same as the

surface plasmon resonance wavelength of the respective core-shell nanoparticle system. So for each system the maximal field enhancement is simulated after excitation at the SPR maximum with air as the surrounding medium. The numerical values of field enhancement near the vicinity of the nanoparticles along the Z-axis, i.e. in the direction of polarization, are on display below the corresponding field maps. It can be observed that the bare Ag nanoparticle and the Ag.L4 core-shell nanoparticle have similar field intensities propagating from the exterior particle surface, but Ag.L8 exhibits a much stronger field within the shell. This is an indication that as the polymer shell thickens, the field becomes localized within the shell, which will result in a drastic loss of the plasmonic enhancement effect near the particle surface. We investigated that the emanating field intensity is not much affected up to a shell thickness of

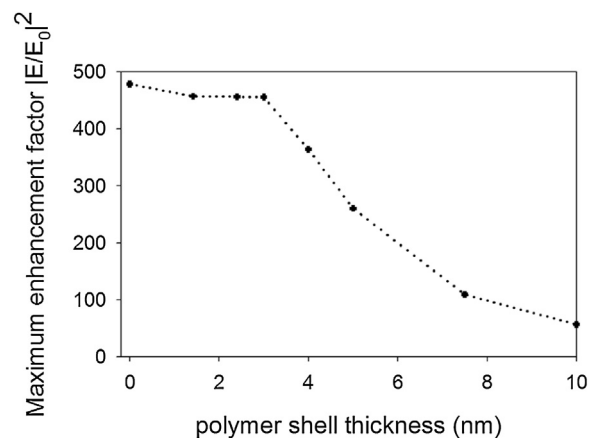


Fig. 6. Effect of polymer shell thickness on maximum enhancement factor near the outer surface of core shell nanoparticle, as determined from finite element simulations.

3 nm, but already drops by ca. 50% for a shell thickness of 5 nm as shown in Fig. 6.

3.3. Long term photocatalytic activity tests

As mentioned before, the main goal of developing these silver core – thin polymer shell nanostructures was to protect the silver nanoparticles against oxidation and clustering when applied on a photocatalytic substrate to be used in an oxygen-rich environment. Silver-modified TiO_2 substrates were prepared by spin

coating 75 μL of the colloidal nanoparticle suspensions onto glass substrates pre-coated with TiO_2 P25 (see experimental section for details). The presence of Ag on the TiO_2 surface was confirmed by HAADF-STEM (EDAX) analysis (Fig. 7). In EDAX measurements a peak at energy 2.983 keV is expected in the presence of Ag. ($\text{Ag L}\alpha = 2.983 \text{ keV}$). At different positions in the sample, a peak for Ag could be observed in the EDX spectrum but unfortunately the amount of Ag deposited was too low for accurate and reliable quantification.

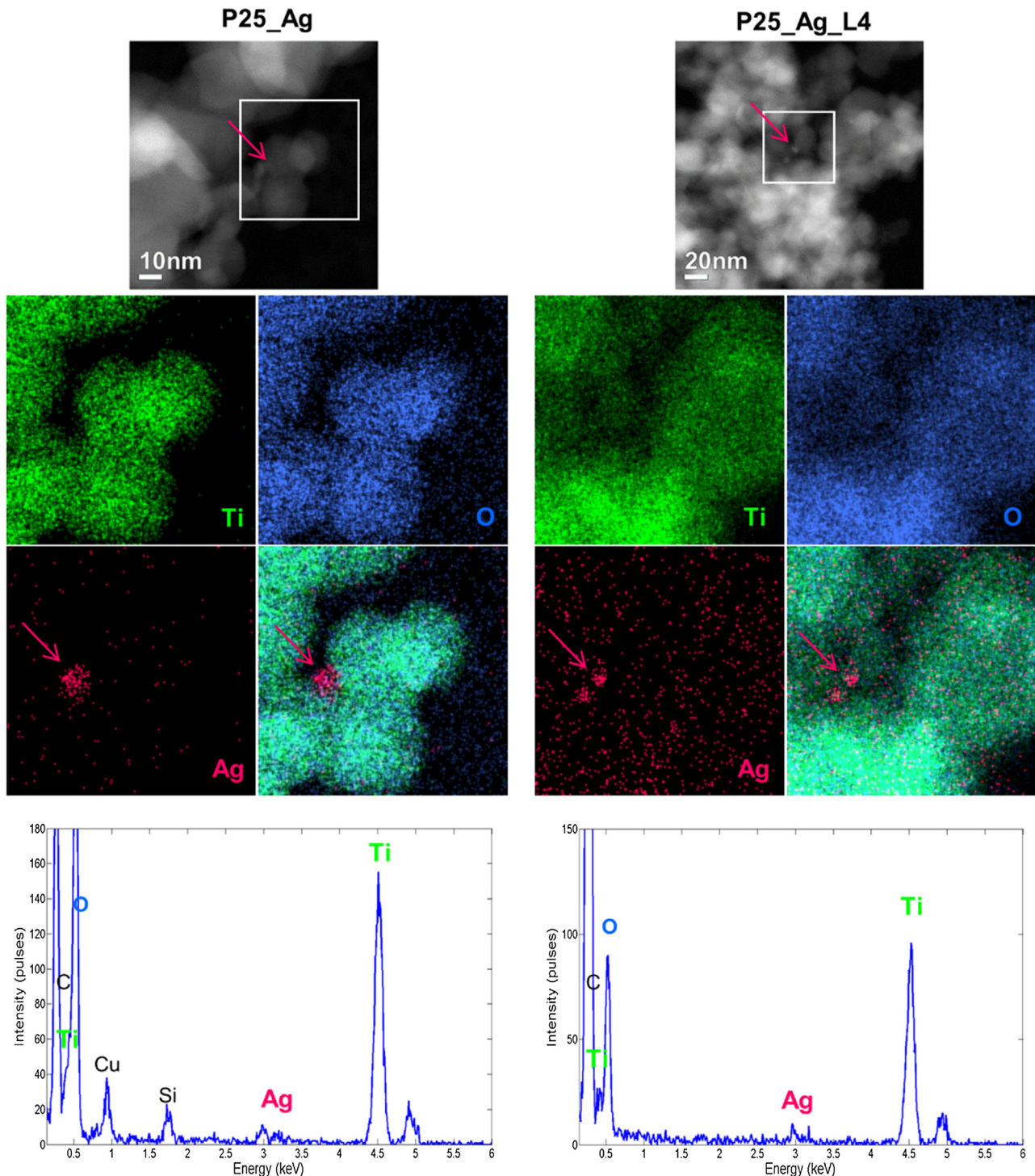


Fig. 7. High angular annular dark field – STEM (HAADF-STEM) images (top) and EDX spectra (bottom) of P25_Ag (left) and P25_Ag_L4 (right) samples. The elemental maps show the presence of the Ag nanoparticles on the surface of TiO_2 .

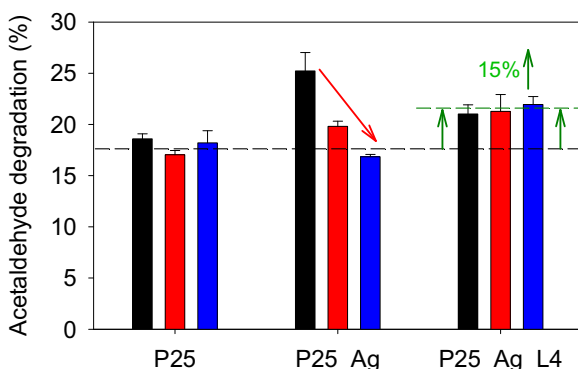


Fig. 8. Long-term photocatalytic activity test. The photocatalytic degradation of gaseous acetaldehyde is evaluated at $t=0$ (i.e. freshly prepared, black), after three weeks (red) and after 16 weeks (blue) of ageing in air. (For interpretation of the references to colour in this figure legend, the reader is referred to the web version of this article.)

To verify the success of the strategy of silver plasmon-enhanced semiconductor photocatalysis, a long-term time study was conducted on the photocatalytic activity of the Ag-TiO₂ plasmonic systems toward the degradation of acetaldehyde in air (Fig. 8). This demanding environmental application was deliberately selected to subject the samples to a stringent oxidative atmosphere in order to verify the effect of the absence and presence of a protective LbL shell, also in the long term. Therefore, a comparison was made between pristine TiO₂ (P25, Evonik), TiO₂ modified with bare Ag nanoparticles and TiO₂ modified with core-shell Ag_L4 nanoparticles. Ag_L4 core-shell nanoparticles were selected as they present the best overlap of the plasmon band and the peak wavelength of the irradiation source used in the photocatalytic experiment (365 nm). This results in a more intense near-field compared to e.g. eight-layered Ag nanoparticles Ag_L8 (Supporting Information Fig. S1) and should consequently result in better plasmonic enhancement [35]. The pristine TiO₂ films retained their activity well over the entire experimental period of 16 weeks, as expected. For TiO₂ films loaded with bare silver nanoparticles (P25_Ag), initially at time $t=0$ (i.e. freshly prepared), a considerable activity enhancement was observed, which can be ascribed to plasmonic enhancement induced by the metallic Ag nanoparticles present on the surface. After three weeks, however, a significant drop in the activity enhancement was observed and no enhancement at all remained after 16 weeks. This effect is attributed to progressive oxidation of the bare Ag nanoparticles, with resulting loss of their plasmonic properties. It has in fact been observed that upon ageing of such systems, a thin diffuse silver oxide (Ag₂O) shell of approximately 2 nm is formed at the nanoparticle surface [36,37]. Its effect on the near field enhancement of the silver nanoparticles is studied by building a finite element model. The simulation demonstrated a 60-fold decrease of the emanating field enhancement for the oxidized silver nanoparticle (supporting Information Fig. S2). This clearly supports the hypothesis that the near-field enhancement drops for oxidized silver nanoparticles resulting in a detrimental loss in plasmonic enhancement of the P25_Ag photocatalyst. In contrast, the system involving Ag nanoparticles protected by a thin polymer shell on TiO₂ (P25_Ag_L4) retained its activity enhancement (15% increase) even after 16 weeks of ageing in air. It should be noted that this plasmonic catalyst has not been optimized towards parameters such as particle size and silver loading. A given set of experimental conditions was arbitrarily chosen and kept fixed for accurate comparative analysis. Therefore the observed increase of 15% is probably not what is maximally attainable and not the goal of this study. Still, the data clearly prove that the thin polymer shell stabilizes the Ag nanoparticles without compromising

the plasmonic properties, making them particularly suited for such demanding applications, even in the long-term.

4. Conclusion

It is shown that the LbL technique is a versatile and highly controllable strategy to prepare core-shell silver nanoparticles encapsulated by a thin layer of polymer with control up to the sub-nanometer level. Furthermore it is demonstrated that PAA can be used as a cost-effective alternative to PSS in this synthesis method with equally good results. The polymer encapsulation protects the Ag nanoparticles from oxidation and clustering, without compromising the plasmon-induced enhancement of the near-field. This was demonstrated by means of finite element simulations and a long-term photocatalytic environmental experiment toward the degradation of acetaldehyde in air. The plasmonic TiO₂ photocatalyst modified with protected Ag nanoparticles retained its activity enhancement of 15% even after 16 weeks of ageing in air, whereas a similar system fabricated with bare Ag nanoparticles lost all of its activity enhancement over this same time period. With this we provide an important step in the development of reliable and durable silver-based plasmonic systems.

Acknowledgements

CD, SL and SWV acknowledge the Research Foundation – Flanders (FWO) for financial support. CD further acknowledges BOF-UGent (GOA 01G01513) and the Hercules Foundation (AUGE/09/014). SB acknowledges the European Research Council for the ERC Starting Grant #335078-COLOURATOM.

Appendix A. Supplementary data

Supplementary data associated with this article can be found, in the online version, at <http://dx.doi.org/10.1016/j.apcatb.2016.06.062>.

References

- [1] H.A. Atwater, A. Polman, Plasmonics for improved photovoltaic devices, *Nat. Mater.* 9 (2010) 205–213, <http://dx.doi.org/10.1038/nmat2629>.
- [2] S. Linic, P. Christopher, D.B. Ingram, Plasmonic-metal nanostructures for efficient conversion of solar to chemical energy, *Nat. Mater.* 10 (2011) 911–921, <http://dx.doi.org/10.1038/nmat3151>.
- [3] S.W. Verbruggen, M. Keulemans, M. Filippoussi, D. Flahaut, G. Van Tendeloo, S. Lacombe, J. a. Martens, S. Lenaerts, Plasmonic gold-silver alloy on TiO₂ photocatalysts with tunable visible light activity, *Appl. Catal. B Environ.* 156–157 (2014) 116–121, <http://dx.doi.org/10.1016/j.apcatb.2014.03.027>.
- [4] S.W. Verbruggen, TiO₂ photocatalysis for the degradation of pollutants in gas phase: from morphological design to plasmonic enhancement, *J. Photochem. Photobiol. C Photochem. Rev.* 24 (2015) 64–82, <http://dx.doi.org/10.1016/j.jphotochemrev.2015.07.001>.
- [5] S.W. Verbruggen, M. Keulemans, B. Goris, N. Blommaerts, S. Bals, J.A. Martens, S. Lenaerts, Plasmonic rainbow photocatalyst with broadband solar light response for environmental applications, *Appl. Catal. B Environ.* 188 (2016) 147–153, <http://dx.doi.org/10.1016/j.apcatb.2016.02.002>.
- [6] K. Awazu, M. Fujimaki, C. Rockstuhl, J. Tominaga, H. Murakami, Y. Ohki, N. Yoshida, T. Watanabe, A plasmonic photocatalyst consisting of silver nanoparticles embedded in titanium dioxide, *J. Am. Chem. Soc.* 130 (2008) 1676–1680, <http://dx.doi.org/10.1021/ja076503n>.
- [7] P. Christopher, D.B. Ingram, S. Linic, Enhancing photochemical activity of semiconductor nanoparticles with optically active Ag nanostructures: photochemistry mediated by Ag surface plasmons, *J. Phys. Chem. C* 114 (2010) 9173–9177, <http://dx.doi.org/10.1021/jp101633u>.
- [8] W. Li, P.H.C. Camargo, L. Au, Q. Zhang, M. Rycenga, Y. Xia, Etching and dimerization: a simple and versatile route to dimers of silver nanospheres with a range of sizes, *Angew. Chemie Int. Ed.* 49 (2010) 164–168, <http://dx.doi.org/10.1002/anie.200905245>.
- [9] J.N. Anker, W.P. Hall, O. Lyandres, N.C. Shah, J. Zhao, R.P. Van Duyne, Biosensing with plasmonic nanosensors, *Nat. Mater.* 7 (2008) 442–453, <http://dx.doi.org/10.1038/nmat2162>.
- [10] S.W. Verbruggen, M. Keulemans, J.A. Martens, S. Lenaerts, Predicting the surface plasmon resonance wavelength of gold-silver alloy nanoparticles, *J.*

Phys. Chem. C. 117 (2013) 19142–19145, <http://dx.doi.org/10.1021/jp4070856>.

[11] M. Liang, S. Angelos, E. Choi, K. Patel, J.F. Stoddart, J.I. Zink, Mesostructured multifunctional nanoparticles for imaging and drug delivery, *J. Mater. Chem.* 19 (2009) 6251, <http://dx.doi.org/10.1039/b902462j>.

[12] D. Radziuk, H. Moehwald, Prospects for plasmonic hot spots in single molecule SERS towards the chemical imaging of live cells, *Phys. Chem. Chem. Phys.* 17 (2015) 21072–21093, <http://dx.doi.org/10.1039/C4CP04946B>.

[13] X. Liu, M. Atwater, J. Wang, Q. Huo, Extinction coefficient of gold nanoparticles with different sizes and different capping ligands, *Colloids Surf. B: Biointerfaces* 58 (2007) 3–7, <http://dx.doi.org/10.1016/j.colsurfb.2006.08.005>.

[14] F. Caruso, Nanoengineering of particle surfaces, *Adv. Mater.* 13 (2001) 11–22, [http://dx.doi.org/10.1002/1521-4095\(200101\)13:1<11::AID-ADMA11>3.0.CO;2-N](http://dx.doi.org/10.1002/1521-4095(200101)13:1<11::AID-ADMA11>3.0.CO;2-N).

[15] G. Schneider, G. Decher, From functional core/shell nanoparticles prepared via layer-by-layer deposition to empty nanospheres, *Nano Lett.* 4 (2004) 1833–1839, <http://dx.doi.org/10.1021/nl0490826>.

[16] G. Schneider, G. Decher, Functional core/shell nanoparticles via layer-by-layer assembly. Investigation of the experimental parameters for controlling particle aggregation and for enhancing dispersion stability, *Langmuir* 24 (2008) 1778–1789, <http://dx.doi.org/10.1021/la7021837>.

[17] O. Tzhayik, P. Sawant, S. Efrima, E. Kovalev, J.T. Klug, Xanthate capping of silver, copper, and gold colloids, *Langmuir* 18 (2002) 3364–3369, <http://dx.doi.org/10.1021/la015653n>.

[18] W. Wang, S. Efrima, O. Regev, Directing oleate stabilized nanosized silver colloids into organic phases, *Langmuir* 14 (1998) 602–610, <http://dx.doi.org/10.1021/la9710177>.

[19] L. Kvítek, A. Panáček, J. Soukupová, M. Kolář, R. Večeřová, R. Prucek, M. Holečová, R. Zbořil, Effect of surfactants and polymers on stability and antibacterial activity of silver nanoparticles (NPs), *J. Phys. Chem. C* 112 (2008) 5825–5834, <http://dx.doi.org/10.1021/jp711616v>.

[20] T.-M. Liu, J. Yu, C.A. Chang, A. Chiou, H.K. Chiang, Y.-C. Chuang, C.-H. Wu, C.-H. Hsu, P.-A. Chen, C.-C. Huang, One-step shell polymerization of inorganic nanoparticles and their applications in SERS/nonlinear optical imaging, drug delivery, and catalysis, *Sci. Rep.* 4 (5593) (2014), <http://dx.doi.org/10.1038/srep05593>.

[21] Y. Zhang, L. Wang, J. Tian, H. Li, Y. Luo, X. Sun, Ag@Poly(m-phenylenediamine) core-shell nanoparticles for highly selective, multiplex nucleic acid detection, *Langmuir* (2011) 2170–2175, <http://dx.doi.org/10.1021/la105092f>.

[22] X. Sun, Y. Li, Ag@C core/shell structured nanoparticles: controlled synthesis, characterization, and assembly, *Langmuir* 21 (2005) 6019–6024, <http://dx.doi.org/10.1021/la050193+>.

[23] J.C. Flores, V. Torres, M. Popa, D. Crespo, J.M. Calderón-Moreno, Preparation of core-shell nanospheres of silica-silver: $\text{SiO}_2@\text{Ag}$, *J. Non-Cryst. Solids* 354 (2008) 5435–5439, <http://dx.doi.org/10.1016/j.jnoncrysol.2008.09.014>.

[24] G. Decher, Fuzzy nanoassemblies: toward layered polymeric multicomposites, *Science* 277 (1997) 1232–1237, <http://dx.doi.org/10.1126/science.277.5330.1232>.

[25] M. Lisunova, M. Mahmoud, N. Holland, Z.A. Combs, M.A. El-Sayed, V.V. Tsukruk, The unusual fluorescence intensity enhancement of poly(p-phenyleneethynylene) polymer separated from the silver nanocube surface by H-bonded LbL shells, *J. Mater. Chem.* 22 (2012) 16745–16753, <http://dx.doi.org/10.1039/C2jm32450d>.

[26] N.G. Bastús, F. Merkoçi, J. Piella, V. Puntes, Synthesis of highly monodisperse citrate-stabilized silver nanoparticles of up to 200 nm: kinetic control and catalytic properties, *Chem. Mater.* 26 (2014) 2836–2846, <http://dx.doi.org/10.1021/cm500316k>.

[27] T. Tytgat, B. Hauchecorne, M. Smits, S.W. Verbruggen, S. Lenaerts, Concept and validation of a fully automated photocatalytic test setup, *J. Lab. Autom.* 17 (2012) 134–143, <http://dx.doi.org/10.1177/2211068211424554>.

[28] S.W. Verbruggen, K. Masschaele, E. Moortgat, T.E. Korany, B. Hauchecorne, J.A. Martens, S. Lenaerts, Factors driving the activity of commercial titanium dioxide powders towards gas phase photocatalytic oxidation of acetaldehyde, *Catal. Sci. Technol.* 2 (2012) 2311–2318, <http://dx.doi.org/10.1039/C2CY20123B>.

[29] S.W. Verbruggen, S. Deng, M. Kurttepeli, D.J. Cott, P.M. Vereecken, S. Bals, J.A. Martens, C. Detavernier, S. Lenaerts, Photocatalytic acetaldehyde oxidation in air using spacious TiO_2 films prepared by atomic layer deposition on supported carbonaceous sacrificial templates, *Appl. Catal. B Environ.* 160–161 (2014) 204–210, <http://dx.doi.org/10.1016/j.apcatb.2014.05.029>.

[30] S. Deng, S.W. Verbruggen, Z. He, D.J. Cott, P.M. Vereecken, J. a. Martens, S. Bals, S. Lenaerts, C. Detavernier, Atomic layer deposition-based synthesis of photoactive TiO_2 nanoparticle chains by using carbon nanotubes as sacrificial templates, *RSC Adv.* 4 (2014) 11648, <http://dx.doi.org/10.1039/c3ra42928h>.

[31] S.W. Verbruggen, S. Lenaerts, S. Denys, Analytic versus CFD approach for kinetic modeling of gas phase photocatalysis, *Chem. Eng. J.* 262 (2015) 1–8, <http://dx.doi.org/10.1016/j.cej.2014.09.041>.

[32] S.W. Verbruggen, M. Keulemans, J. van Walsem, T. Tytgat, S. Lenaerts, S. Denys, CFD modeling of transient adsorption/desorption behavior in a gas phase photocatalytic fiber reactor, *Chem. Eng. J.* 292 (2016) 42–50, <http://dx.doi.org/10.1016/j.cej.2016.02.014>.

[33] P.B. Johnson, R.W. Christy, Optical constants of the noble metals, *Phys. Rev. B* 6 (1972) 4370–4379, <http://dx.doi.org/10.1103/PhysRevB.6.4370>.

[34] K.-H. Kyung, K. Fujimoto, S. Shiratori, Control of structure and film thickness using spray layer-by-layer method: application to double-layer anti-reflection film, *Jpn J. Appl. Phys.* 50 (2011) 035803, <http://dx.doi.org/10.1143/JJAP.50.035803>.

[35] D.B. Ingram, P. Christopher, J.L. Bauer, S. Linic, Predictive model for the design of plasmonic Metal/Semiconductor composite photocatalysts, *ACS Catal.* (2011) 1441–1447.

[36] Y. Han, R. Lupitsky, T.M. Chou, C.M. Stafford, H. Du, S. Sukhishvili, Effect of oxidation on surface-enhanced raman scattering activity of silver nanoparticles: a quantitative correlation, *Anal. Chem.* 83 (2011) 5873–5880, <http://dx.doi.org/10.1021/ac2005839>.

[37] R. Sachan, V. Ramos, A. Malasi, S. Yadavali, B. Bartley, H. Garcia, G. Duscher, R. Kalyanaraman, Oxidation-resistant silver nanostructures for ultrastable plasmonic applications, *Adv. Mater.* 25 (2013) 2045–2050, <http://dx.doi.org/10.1002/adma.201204920>.